JAST, Vol. 14, No. 2, pp. 52-65

JAST
Journal of Aerospace Science and Technology

Science – Research Article

A New Method to Primary and Optimized Design of Ducted Fan

Ahmad Sharafi

Shahid Sattari Aeronautical University of Science and Technology

*Email: **sharafi@ssau.ac.ir**

In the present study, the aerodynamic performance of the ducted fan is investigated using the surface vorticity method and the lifting line theory. In the previous researches, to investigate most of the duct parameters, the empirical tests and/ or the computational fluid dynamics simulation approaches are applied. Our goal is to present a new method for considering the effects of the duct on the fan enclosed in a duct. In this method, the lift and drag coefficients are the only input parameters. The present method requires considerably less computational time than the CFD methods. Also, the aerodynamic optimization of the fan blades geometry has been carried out using particle swarm optimization method (PSO) to achieve the optimum blade geometry and the maximum output power. The results of this method are in excellent agreement with the experimental data in references. By optimizing the geometry of the blade, the output power of the ducted fan is increased 10 percentages in comparison to the ducted fan with old blade geometry.

Keywords: *Ducted Fan, Surface Vorticity Method, Lifting Line Theory, Optimization*

Nomenclature

A : Cross sectional area (m2)
B : Number of blades (-)
c : Blade chord (m)
c_d : Sectional drag coefficient (-)
c_l : Sectional lift coefficient (-)
K : Coupling Coefficient (-)
p : Pressure (N.m-2)

Greek letters

α : Angle of attack (rad)
β : Viscosity (Pa. s)
γ : Vorticity strength per unit length (m.s-1)
ρ : Density (kg.m-3)
ϕ : Angle of relative wind (rad)
ω : Local Rotational Speed (rad.s-1)
Ω : Rotor rotational speed (rad.s-1)
Γ : Vorticity strength (m2.s-1)
σ : Source strength (m.s-1)

Subscripts

duct : Applied on duct
hub : Applied on hub
ind : Induced
m : Location m
n : Location n
te : Trailing edge
∞ : Free stream

Superscripts

1- * : Dimensionless

2- --- : Temporal average

Introduction

At the ducted or shrouded propeller, the duct increases the inlet velocity of wind on the blade and the rotor converts power into thrust by rotating the blades around a shaft. The blades should be modified by considering the flow interactions, due to the effect of the duct on the flow field. Besides, the shape of the duct is one of the important items which contribute to the efficiency of ducted fans.

1. Lecturer

Received: 27 Jan. 2021
Accepted: 12 June 2021

It is usually axisymmetric with an airfoil cross-section. This type of duct can provide additional thrust. The investigations in the propeller field, showed the possibility of increasing efficiency of wind power using the duct which surrounding the blades. Shrouded fans are useful technologies that have higher efficiency compared to conventional fans. Also, using a ducted fan is economical for small and large applications. The field of ducted/shrouded propeller was developed during the attempts of researchers to improve the performance of propellers [1].

It has been proven that using duct around propellers can exceed the Betz limit [2]. The ducted fan has more benefits in comparison with bare fans including enhanced air mass flow rate [2-4], lower fluctuating blade loads [2], less noise [2,5], lower cut-in wind speeds [6], less sensitivity to turbulence [6], better resistance to fatigue [6], higher possible rotational speed [7], and reduction in tip losses [8].

Ludwig Kort patented the first form of ducted fan in 1924. He used the rotor in a long duct for marine applications. Later, because of the disadvantages of using long channel such as frictional resistance, nozzle shaped ducts were replaced. Stipa and Kort have investigated the effect of the presence of a nozzle on the efficiency of ducted propellers [9, 10]. They found that ducting the fan increases the efficiency of the fan.

Although, for many decades, the design and analysis of ducted fans were mainly investigated experimentally [11-15], several numerical and analytical methods have also been developed since 1940 [16, 17]. Most of these works were generally based on the combination of the velocity field induced by the duct and rotor.

Kruger investigated different ducted fan configurations, including fifteen different duct cross-sections and two types of fans [18]. He observed the advantages of the ducted fan compared to a free propeller and also illustrated experimentally that the wake diameter behind the rotor of a ducted fan is a function of the duct geometry and not the fan.

Ko et al. developed a numerical code, for the purpose of the initial design of a ducted fan [19]. They concluded that the results of their code were in good agreement with other experimental data. Zhao and Bil numerically investigated ducted fan UAV using computational fluid dynamics to develop an aerodynamic model based on various speeds and angles of attack [20].

Abrego and Bulaga carried out an experimental test to study the flow characteristics and to investigate the influence of the flap chord length on the performance of ducted fans [21].

Ahn and Lee, based on their numerical investigations, identified the effective parameters which influence the design process and performance analysis of the ducted fan [22]. They used stream surface axisymmetric analysis to consider physical characteristics and to propose the design method of the ducted fan.

Besides these studies, various inviscid methods have been used to analyze different types of ducted fans. Kerwin et al. introduced a new method to evaluate the performance of the ducted propeller by combining a panel method with a vortex lattice method [23]. In this study, the influence of the panel arrangement and tip clearance was investigated. Following this work, Hughes also applied a panel method to a ducted propeller to assess the effect of tip clearance on the efficiency of a propeller enclosed in a duct [24].

By comparing the results of a panel method with the experimental works and also RANS simulations, it can be concluded that by considering the viscous effects, this method has acceptable accuracy in analyzing the ducted fans [25, 26].

Lind et al. [27] numerically investigated a ducted fan using a panel method, and their results were in good agreement with the experimental investigation of Martin and Tung [28]. Graf et al. [29] improved the ducted fan performance with a new design of leading-edge geometry. They considered the effects of the adverse aerodynamic characteristics in the design procedure. He and Xin [30] developed ducted fan models using an unsteady ring-vortex method and the blade element theory for the duct and the fan, respectively.

Both linearized and non-linear actuator disk methods are the oldest methods used in the field of bare and ducted fans [31-33]. There are some examples of using the actuator disk method to analyze ducted propellers [34-37].

Although many analytical models have been developed to describe the performance of the ducted fan, all of these models require some parameters which arise from experimental tests or computational fluid dynamic (CFD) simulations to consider the effects of the duct on the fan [36-39]. The present method with a considerable reduction in computational costs requires only lift and drag

coefficient as an input of the proposed method. In addition, this method is combined with the Particle Swarm Optimization (PSO) method to improve the output performance of the ducted fan. In other words, the presented method designs the best shape of blades for any considered duct and in any conditions. Reducing the computational costs and also considering the effects of the duct on the rotor and its performance using the vorticity method are the innovations of this work.

Methodology

Potential flow around simple two-dimensional objects, such as a "Rankine" body, an ellipse, Joukowski airfoils, etc., can be obtained by superposition of uniform flow, sources, sinks, and doublets, or through the conformal mapping. However, in practical applications, it is often necessary to simulate the flow around the bodies which have complicated configurations.

In the present study, the surface vorticity distribution technique has been used to represent both the duct and the hub. This portion of the theory has been developed from similar two-dimensional theories which have been proved to be successful for other applications. The present method makes use of the established lifting line theory for the rotor. Furthermore, some modifications have been made to allow for its combination with the duct theory.

In this method, vortex sheets are used to define the duct shape and to consider the flow changes across the fan disk. A potential flow method can be used to describe the flow of a ducted fan. According to the Betz model, by assuming the uniform changes in pressure across the fan disk, both regions of the flow have a potential function [40]. Lewis used vortex methods to analyze lifting airfoils problems [41].

Surface vorticity method

The surface vorticity method is the most direct model for the numerical investigation of the potential flow about bodies. This method, is initially proposed by Martensen [42] and then extensively used by Lewis [41, 43]. According to this method, the surface of the body is replaced by a finite number of vorticity sheets.

The axisymmetric induced velocity at a point m due to a small vorticity element of vortex filament L_n of strength Γ_n at a point n with a radial distance r_{mn} is obtained from the Biot-Savart law.

$$dq = \frac{\Gamma_n dl_n \times r_{mn}}{4\pi {r_{mn}}^3} \quad (1)$$

The velocity of the flow on and parallel to the surface is zero at m (Dirichlet boundary). By considering this boundary condition:

$$-\frac{1}{2}\gamma_m + \frac{1}{4\pi}\iint_S \frac{i_m \times \left(\left(\gamma_n \times r_{mn}\right) \times i_m\right) ds}{r_{mn}^3} = \quad (2)$$

Decomposing the induced velocity (q) into its components yields the following:

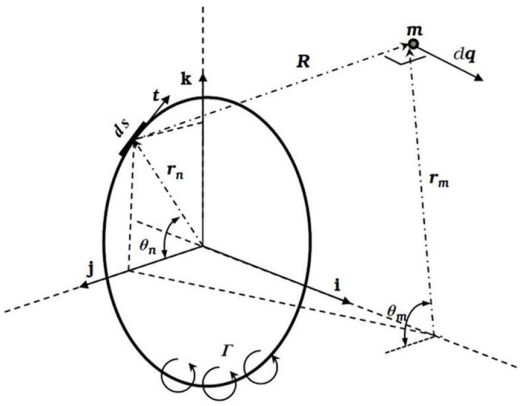

Fig. 1. Vortex Ring in axisymmetric surface vorticity method [41]

$$u_{mn} = \frac{1}{4\pi}\int_0^{2\pi} \left\{ \frac{r_n - r_m \cos(\theta - \theta')}{\left[(x_m - x_n)^2 + {r_n}^2 + {r_m}^2 - 2r_n r_m \cos(\theta - \theta')\right]^{\frac{3}{2}}} \right\} \kappa$$
$$v_{mn} = \frac{1}{4\pi}\int_0^{2\pi} \left\{ \frac{(x_m - x_n)\cos\theta'}{\left[(x_m - x_n)^2 + {r_n}^2 + {r_m}^2 - 2r_n r_m \cos(\theta - \theta')\right]^{\frac{3}{2}}} \right\} \kappa \quad (3)$$

Boundary layer

The concept of the boundary layer developed by Prandtl in 1904 provides an essential link between the ideal and the real fluid flow [44].

According to the fluid viscosity, in all real flows, a boundary layer is created adjacent to the surface of the body. In this procedure, in order to consider the effects of the boundary layer, the surface of the body is covered with numerous vortices. In this layer, sufficient number of vortices are applied to reduce the fluid velocity from a certain value

outside the shear layer to zero at the surface of the body.

If Reynolds number approaches infinity and viscosity approaches zero, the viscous diffusion of normal on the body surface would also reduce and as a consequence, the boundary layer would become infinitely thin. In practice, the boundary layer can thus be represented by an infinitely thin vorticity sheet with a velocity discontinuity across it. The velocity distribution can be obtained, using the body surface vorticity (Fig. 2).

The total circulation of the vorticity element around *abcd* can be defined as,

$(v_{s_o} - v_{s_i})ds = \gamma(s)ds$

Where v_{s_o} and v_{s_i} are the fluid velocities parallel to the surface just outside and inside the vortex sheet, respectively. Because of the viscous forces in the boundary layer, the no-slip condition is applied to satisfy the zero velocity on the body surface ($v_{s_i} = 0$). If the turbulence of the boundary layer and the flow separation, which may occur at high Reynolds numbers, were neglected, it can be considered in the proposed theory as an irrotational potential flow. Therefore, it can be concluded that the vorticity model could effectively simulate the physics of a real fully attached high Reynolds number flow.

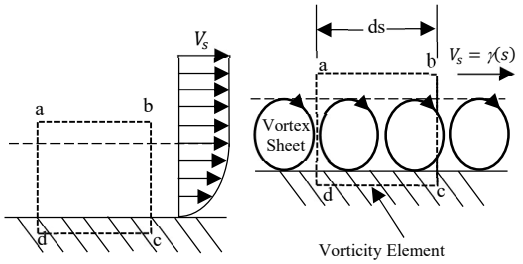

Fig. 2. Boundary layer and vortex equivalent [45]

The coupling coefficient linking elements *m* and *n* then becomes:

$$\bar{K}(s_m, s_n) = u_{mn}\cos\beta_m + v_{mn}\sin\beta_m \quad (4)$$

In this equation, β_m is the body profile slope.

$$\beta_m = \arctan(dr/dx) \quad (5)$$

By representing the body with M vortex rings, the potential flow is obtained by:

$$\sum_{n=1}^{M} \bar{K}(s_m, s_n)\gamma(s_n)\Delta s_n = -W\cos\beta_m \quad (6)$$

Where

$$K(s_m, s_n) = \bar{K}(s_m, s_n)\Delta s_n \quad (7)$$

And $\gamma(s_n)\Delta s_n$ is the surface vorticity element.

The self-induced coupling coefficient is also obtained from:

$$K(s_m, s_m) = -\frac{1}{2} + \frac{\Delta s_m}{4\pi R_m} - \frac{\Delta s_m}{4\pi R_m}\left[\ln\frac{8\pi r_m}{\Delta s_m} - \frac{1}{4}\right]\cos\beta_m \quad (8)$$

Where R_m and r_m are the two radius of curvatures possessed by a ring vorticity element in the (x,r) and (r,θ) plane, respectively. Then the induced velocities can be calculated as follows:

$$u_{mn} = -\frac{1}{2\pi r_n\sqrt{\left[x^2 + (r+1)^2\right]}}\left\{K(k) - \left[1 + \frac{2(r-1)}{x^2 + (r-1)^2}\right]E(k)\right\}$$
$$v_{mn} = -\frac{x/r}{2\pi r_n\sqrt{\left[x^2 + (r+1)^2\right]}}\left\{K(k) - \left[1 + \frac{2r}{x^2 + (r-1)^2}\right]E(k)\right\} \quad (9)$$

In these equations, $K(k)$ and $E(k)$ are the first and the second kind elliptic integrals and:

$$x = \frac{x_m - x_n}{r_n},\ r = \frac{r_m}{r_n},\ \mathrm{k} = \sqrt{\frac{4r}{x^2 + (r+1)^2}} \quad (10)$$

For computational analysis, Eq. (6) becomes a set of linear equations:

$$\begin{pmatrix} K_{11} & K_{12} & K_{13} & \cdots & K_{1M} \\ K_{21} & K_{22} & K_{23} & \cdots & K_{2M} \\ K_{31} & K_{32} & K_{33} & \cdots & K_{3M} \\ \cdot & \cdot & \cdot & \cdots & \cdot \\ K_{M1} & K_{M2} & K_{M3} & \cdots & K_{MM} \end{pmatrix} \begin{pmatrix} \gamma(s_1) \\ \gamma(s_2) \\ \gamma(s_3) \\ \cdot \\ \gamma(s_M) \end{pmatrix} = \begin{pmatrix} rhs_1 \\ rhs_1 \\ rhs_1 \\ \cdot \\ rhs_M \end{pmatrix} \quad (11)$$

To obtain a non-singular matrix and the correct answer, the following corrections should be applied to the above set of equations:

To determine the magnitude of the circulation around the body, the Kutta condition should be applied on the sharp edge. This condition states that the velocity is finite because the trailing-edge angle is finite ($\gamma(s_{te}) = -\gamma(s_{te+1})$) [46].

The self-induction for airfoil curvature ($k(s_m, s_n) = 0$).

A back diagonal correction is another important correction which needs to be applied on Eq. (11) to obtain a non-singular matrix ($\gamma(s_m)\Delta s_m = 0$).

From the vorticity distribution around the diffuser, the pressure coefficient is obtained by:

$$C_p = \frac{P - P_\infty}{\frac{1}{2}\rho U_\infty^2} = 1 - \left(\frac{\gamma(s)}{U_\infty}\right)^2 \quad (12)$$

Lifting line theory

The Lifting line theory is used to model the rotor and wake of a fan. In other words, the fan blades are replaced by lifting lines and trailing edge vortices that shed along the blade span. Helmholtz was the first to make use of the vortex filament concept in the analysis of inviscid incompressible flow. Helmholtz's vortex theorem state that the vortex filament cannot end in a fluid; it must extend to the boundaries of the fluid or form a closed path (Fig. 4). According to this theory, the wake is assumed to extend 8 rotor diameters downstream of the rotor. After this, it is assumed that the wake influence is negligible. This is to approximate the rotor wake extending to infinity downstream of the rotor.

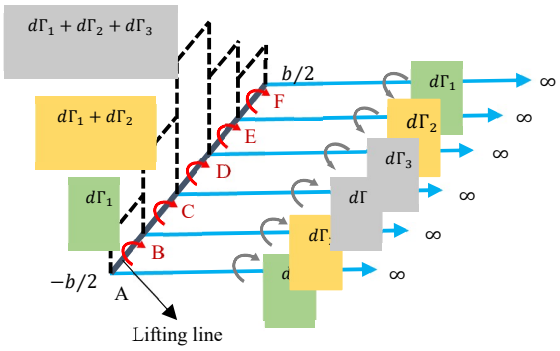

Fig. 3. Lifting line theory

The vortex in Fig.4 is in the shape of horseshoe, and is also called a horseshoe vortex.

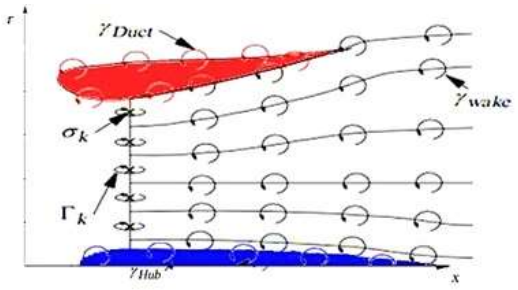

Fig. 4. Vortex distribution

The current method tries to calculate the effect of the duct on the flow field as well as the effect of the rotor on the flow. The method is programmed in MATLAB software, and the pseudo-code of the implemented method is shown in Fig. 5. In this method, the duct, the hub and rotor geometry, and the operating conditions, including the free stream velocity, the rotor RPM, the global pitch angle, and the air density are the inputs. The chord and pitch angle of the blade and also the lift and drag coefficients are the other input parameters. Using the XFOIL program, the sectional lift and drag coefficients are obtained.

Start

1. *Import initial data*
2. *Import and generate geometry*
3. *Calculate influence coefficients*
4. *Solve surface vorticity distribution without rotor*
5. *Calculate inflow condition based on surface vorticities*
6. *Calculate blade circulation and source strengths from airfoil data*
7. *Calculate wake vortex sheet strength*
8. *Calculate surface vorticity distribution*
9. **If** *error of comparison between new distribution and old distribution can be ignored*
10. **Go to** line 14
11. **Else**
12. *Update surface vorticity*
13. **Go to** *line 5*
14. *Calculate Power and Thrust*

Fig. 5. Pseudo code of proposed method

Effects of duct, hub and rotor on the incoming flow are the most important part in analyzing a ducted fan. The duct and hub influence on the flow is calculated using the axisymmetric surface vorticity method. The rotor is then modeled using a blade lifting line theory.
The geometry is approximated by linear panel elements to calculate the body influence coefficients. The length of these panels is calculated by:

$$\Delta s_n = \sqrt{\left(x_{n+1} - x_n\right)^2 + \left(y_{n+1} - y_n\right)^2} \qquad (13)$$

Where, the profile slope is:

$$\arctan \beta_m = \frac{y_{n+1} - y_n}{x_{n+1} - x_n} \qquad (14)$$

Using Eq. (7), the coupling coefficients are then calculated. The wake is approximated to the duct and hub geometry with the initial vortex strength of zero. Then the wake influence is assumed neglected to approximate the rotor wake extending to the infinity downstream of the rotor. The velocity distribution at the rotor plane is obtained using the coupling coefficients of the duct, the hub,

and the wake. These induced velocities are then used to determine the circulation for each blade segment. After this, the strengths of the sectional blade shed vortices can be calculated using the circulation of the blade sections. The wake and rotor effects are then updated and the velocity at the rotor plane can also be updated using newly updated surface vorticity strengths. This iterative process continues until the surface vorticity strengths converge within a reasonable tolerance.

The effect of the blade drag can also be taken into account by considering the blade as a source sheet. Finally, the potential flow system of equations about the axisymmetric geometry is given as follows:

$$\begin{pmatrix} K_{HubHub} & K_{HubDuct} \\ K_{DuctHub} & K_{DuctDuct} \end{pmatrix} \begin{pmatrix} \gamma(s_1) \\ \cdot \\ \cdot \\ \gamma(s_M) \end{pmatrix} + K_{wake}\gamma_{wake} + K_{blade}\sigma_{blade} = \begin{pmatrix} rhs_1 \\ \cdot \\ \cdot \\ rhs_M \end{pmatrix} \quad (15)$$

Where σ_{blade} is the strength of the blade source sheet. The total axial velocity at the rotor plane which consists of free stream velocity and the induced velocities is then calculated by:

$$U_{rotor} = U_{\infty} + U_{ind,DuctHub} + U_{ind,vortex} \quad (16)$$

The elemental axial force of a rotor with B blades is then given by:

$$dF = \frac{1}{2} B \rho U_{rel}^2 \left(c_l \cos\phi + c_d \sin\phi\right) c dr \quad (17)$$

The elemental torque is also given by:

$$dQ = \frac{1}{2} B \rho U_{rel}^2 \left(c_l \sin\phi - c_d \cos\phi\right) c r dr \quad (18)$$

The output power of the system is then calculated as follows:

$$P = \int_{R_{Hub}}^{R_{Duct}} \Omega dQ \quad (19)$$

Where Ω is the rotor angular velocity.

Optimazation

An Optimization is the decision processes which choose the best decision between various alternatives. An optimum fan is one of the main goals of the fan design. The power output of a fan is directly influenced by its aerodynamic performance. The aerodynamic optimization of the blade depends on geometric optimization since the various shapes of the blade section have different aerodynamic forces, and consequently, its performance is affected by these different geometries.

Global optimum design can be achieved through those methodologies, where each blade analysis requires a CFD computation, which can make this process computationally expensive, and thus time-consuming. The high computational costs for these approaches have motivated proposals for modified algorithms or other alternatives for faster methodologies.

Kennedy and Eberhart developed the Particle Swarm Optimization based on swarm intelligence, such as population movements of birds in nature [47]. This nature-inspired algorithm has the random searching ability and has been widely used for geometrical optimization. In PSO, each particle can be shown by its velocity and position; the particles fly through the problem space according to the current global best and their own best location in history (Fig. 6) [48].

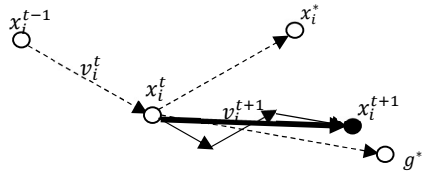

Fig. 6. Schematic of the motion of a particle in PSO algorithm

The movement of a particle in the PSO algorithm depends on a stochastic component and a deterministic component. In other words, a pattern-search-type mutation defines the new position of a particle.

The velocity and the position of each particle are obtained from equations (20) and (21), respectively [48].

$$v_i^{t+1} = w v_i^t + \alpha\varepsilon_1\left[g^* - x_i^t\right] + \beta\varepsilon_2\left[x_i^* - x_i^t\right] \quad (22)$$

$$x_i^{t+1} = x_i^t + v_i^{t+1} \quad (23)$$

Where ε_1 and ε_2 are two random vectors and these values are also between 0 and 1. The parameters α and β are the learning parameters, which are approximately equal to two, $\alpha \approx \beta \approx 2$.
Table 1 illustrates the definition of parameters in the PSO algorithm.

Table 1. Definition of parameters in the PSO algorithm

Parameter	Definition	Parameter	Definition
x_i^t	Previous position of particle i	x_i^{t+1}	Current position of particle i
v_i^t	Previous velocity of particle i	v_i^{t+1}	Current velocity of particle i
x_i^*	Own best location in history	g^*	Current global best
α & β	Learning parameters	ε_1 & ε_2	Random vectors
w	Inertia weight		

The right-hand side of equation 22 consists of three terms: inertia, personal influence, and social influence, respectively. Each term has a specific influence on the swarm movement of a particle.
Inertia: Particle moves in the same direction and with the same velocity.
Personal Influence: If the current position is not better than the previous one, particle returns to a previous position.
Social Influence: Particle searches to find the best neighbor's direction and then tries to follow it.

$$w = \frac{2}{\left|2 - \varphi - \sqrt{\varphi^2 - 4\varphi}\right|} \quad (24)$$

In PSO method, many variables can improve this optimization algorithm. One of these variables is the inertia weight (w) in equation (22), which enhances the capacity of exploring solution space [49]. The value of this parameter indicates the influence rate of the particle velocity of their speed in the previous repetition. Bansal et al. have collected and examined various functions of some references for inertia weight [50]. The reference [51] also describes selection of this parameter and its effect on the speed of optimization. The low value of inertia weight increases local search, and its large value increases the search for the entire range of solutions. In fact, by choosing the value of this quantity, we specify that the focus of the search is on local search or global search within the defined range. Usually, the massive inertia weight is initially used and its value is gradually decreased. The value of this parameter is initially considered to be between 0.8 and 1.2 [51].
The PSO algorithm is combined with the potential flow method to achieve the optimum blade geometry and the maximum output power (Fig. 8). The magnitude of the chord and the twist angle are selected as a variable parameter. We can geometrically optimize the cross-sections of the blade.

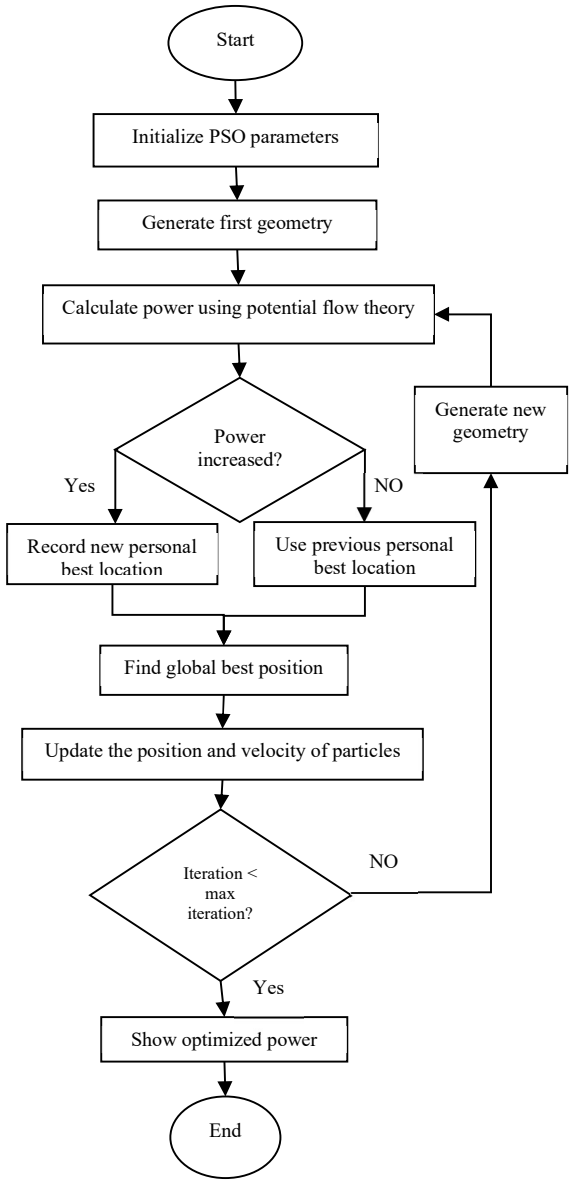

Fig. 7. The selected sections to optimization

The position of the selected sections is the same as the position of the primary blade (13 sections).

Therefore, each particle in the PSO algorithm is a matrix with 13 rows and 2 columns, including the magnitude of the chord and the twist angle of the blade in different sections (Fig. 8).

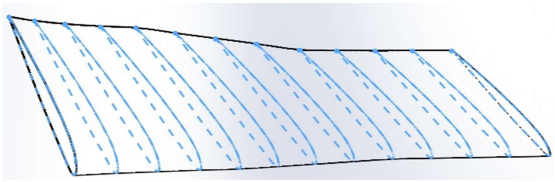

Fig. 8. The selected sections to optimization

This matrix is generated randomly in code, and then the output power of generated geometry is obtained from the potential flow algorithm (Fig. 5). At each iteration, the newly obtained output power is compared with the old value. This procedure continues until the best geometry of blade, which has the maximum output power, is obtained.

The upper and lower bonds of the chord and twist distributions are presented in Table 2.

Table 2. Upper and lower bonds of optimization process

Variables	Upper bond	Lower bond
Chord	0.1	0.25
Twist	0	30

Validation

The Donqi Urban Ducted Fan is selected to validate the current method. As it shows in Fig. 9, the DONQI is a diffuser augmented fan with an annular wing as a diffuser. Several experimental studies are done in the past with this kind of shrouded propeller [5].

Fig. 9: DONQI Ducted Fan [52]

The pressure difference between the two sides of the blade causes the circulation around the wing, which leads to the lift force. According to the Biot-Savart law, this circulation is a reason for an increase of the velocity at the throat section of the duct. Also, it will be the main reason for increasing the efficiency of ducted fans. The main characteristics of the DONQI fan are shown in table3 [52].

Table 3. Specification of the DONQI fan [52]

Parameter	Value
Maximum power [kW]	2.25
Cut-in wind speed [m/s]	2.5
Cut-out wind speed [m/s]	30
Number of Blades	3
Airfoils	NACA 2207
Rotor diameter [m]	1.5
Diffuser diameter [m]	2

The wake mesh dependency test is investigated at a wind speed of 7 m/s and 400 RPM (Fig. 10). As it is illustrated, the solution converges when the number of wake segments is greater than 300. Increasing the wake segment past this only increases the calculation time without any effects on accuracy. Therefore, it is not recommended to use more than 300 wake segments in the analysis.

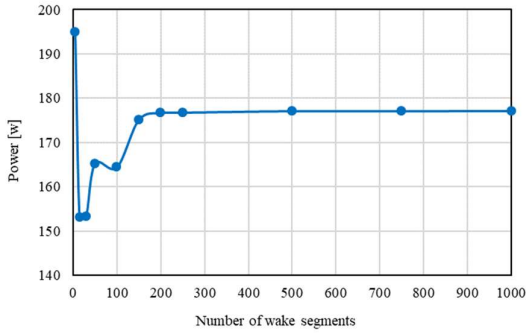

Fig. 10. Wake mesh dependency test

The surface vorticity method using 64 elements is applied on NACA 662-015 annular airfoil to obtain the surface pressure distribution. Fig. 11 shows the numerical results of this method in comparison with the experimental data given in reference [45]. As can be seen, both the numerical and the experimental pressure distribution have the same trend. Also, solutions are in excellent agreement for both lower and upper surfaces.

However, for a streamlined body like an airfoil, at a small angle of attack, the flow will not separate. Potential flow theory can predict such flow field significantly well.

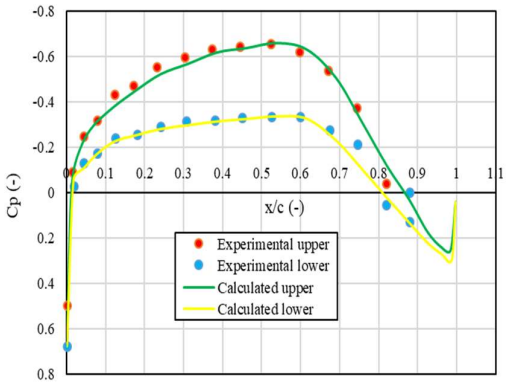

Fig. 11. Numerical and experimental surface pressure distribution on NACA 662-015

Fig. 12 shows the numerical and the experimental pressure distributions over the suction side and the pressure side of the diffuser. The pressure distributions are for a case without a rotor. It indicates that both graphs have the same trend except for the position where the experimental result has a sharp peak. The experimental data is obtained by Ten Hoopen [53]. In this reference, it is mentioned that the installation of a noise damper rim which is not fully aligned with the surface of the duct caused a peak at 0.3 chords in the experimental result. Because of this bump, the flow will separate resulting in a sudden pressure increase.

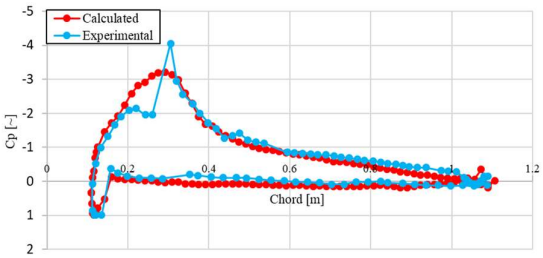

Fig. 12. The pressure distributions over the surface of the diffuser for a duct without a rotor

Results and discussions

One of the main advantages of enclosing fan in the duct is increment of velocity at rotor plane. The normalized velocities at rotor plane are shown at Fig. 13 according to the radial position. There is a direct link between the inlet velocity and the velocity at rotor plane. The normalized velocity is increased along the blade due to the effect of angular velocity which has maximum value at the tip of blade. The reason to changing the slope of the curves for different velocities is the effect of annular velocity on the total velocity of rotor.

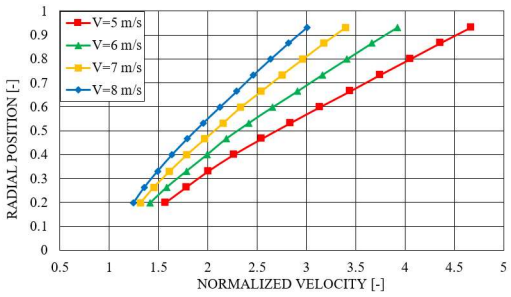

Fig. 13. Normalized velocity at rotor plane of ducted fan

The power curve is created by obtaining the maximum power at each velocity for various RPMs. Comparison of the calculated and the experimental power curve is shown in Fig. 14. Results show that this method has more accuracy for higher velocity and as it is expected, overpredicts the calculated power.

The red graph in Fig. 14 is the aerodynamic power of the rotor and not the output electrical power by the generator. It does not consist of the mechanical and the electrical efficiencies of the gearbox and the generator of the fan. The mechanical and the electrical efficiencies were not explicitly defined for the experimental data provided in the related reference.

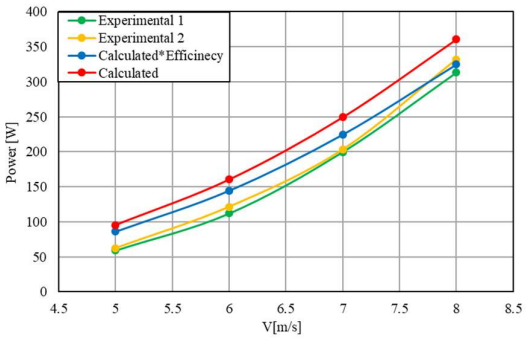

Fig. 14. The power curve of ducted fan

However, in the other references, it is reported that the typical gearbox efficiencies

are on the order of 95 to 98 percent and also the efficiency of the generator is typically on the order of 90 to 95 percent. Finally, to consider the effect of them in the results, we consider a mechanical and electrical efficiency of 0.9 [54]. By considering this efficiency, the numerical results (blue graph) are closer to the experimental data. These slight differences between the obtained power and the experimental results show the accuracy of the model. The accuracy of the model in higher velocities is more than lower velocities.

It is mentioned that the global blade pitch is possible to vary by +/- 1 degree [52]. To see the effect of these sources of error, the power curve of a ducted fan for the different global pitch angle is indicated in Fig. 15. This figure shows that by changing 1 degree in global blade pitch, the power can be changed considerably.

Fig. 15 shows that an increase in the blade angle will reduce the power output, especially at a higher RPM and a reduction in the global blade angle will increase the power output.

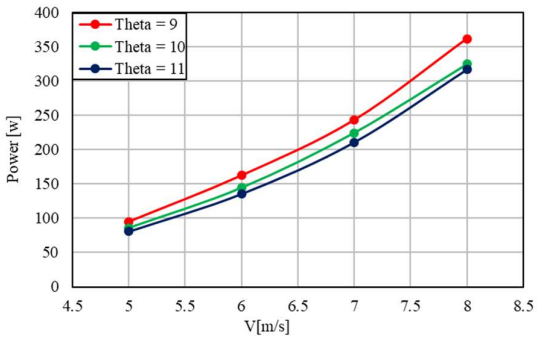

Fig. 15. The Power curve of the ducted fan for the different global pitch angle (9, 10 and 11 degrees)

To illustrate the effect of placing a duct around the fan on the output power, its power curve s plotted in Fig. 16. The duct radius is assumed to be very large to simulate a bare fan with the proposed method. In other words, by considering the duct radius to be very large, the effect of the duct is ignored. The performance of the bare fan is increased by approximately 27 percentages with the addition of fan.

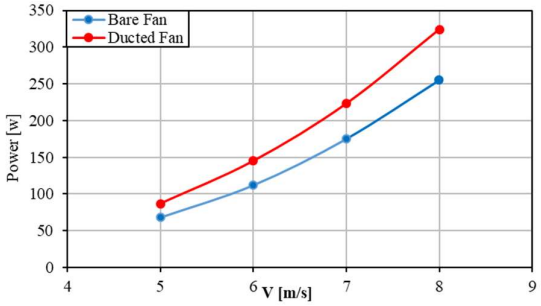

Fig. 16. The power curve of the ducted fan compared to the bare fan

In addition, the thrust curves which contain the maximum thrust at each velocity inlet are shown in Fig.17.

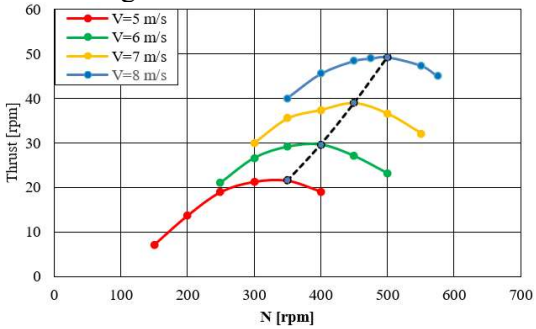

Fig. 17. The Thrust of the ducted fan at different inlet velocity

Fig.18 indicates the torque that is produced by the ducted fan at different velocities. The effect of inlet velocity on the angular velocity at the rotor plane could be observed in this graph. The torque curve is also reported in this figure.

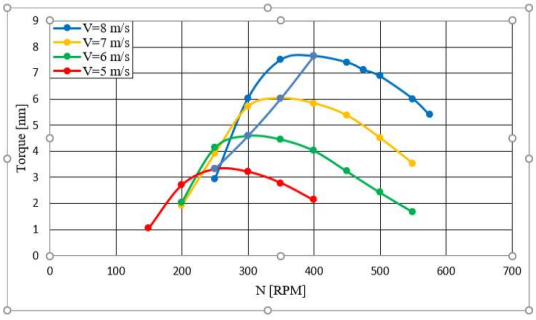

Fig. 18. The Torque of the ducted fan at different inlet velocity

Fig. 19 indicates the chord length distribution of the old and the optimized blade. There is a noticeable increase in the chord length at the root. The optimal blade has a very wide root section compared to the old blade. The increased root section can cause some

limitations for manufacturing the blade, to reduce these limitations the design should be linearized.

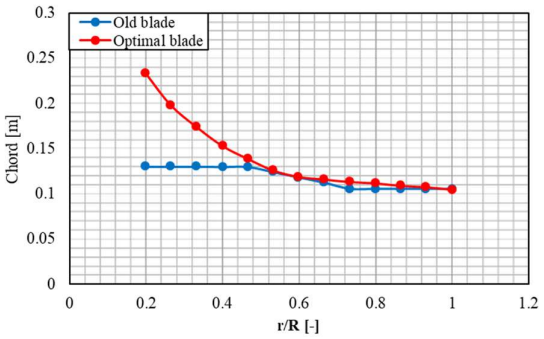

Fig. 19. The chord length of the optimized blade compared to the old blade

The effect of optimization on the chord length is obtained as bellow:

$$\frac{c_{root,optimized\ blade}}{c_{root,old\ blade}} = 1.79$$

A bigger chord at the root of the optimal blade is the reason of a lower cut-in speed. The lower cut-in speed depicts that the wind speed at the rotor plane is greater than the free stream wind speed.

Another point is that the axial velocities for the old blade in a higher tip speed ratio are lower for the optimal blade. This can lead to a lower thrust in a lower power coefficient.

The twisted angle of the old blade and the redesigned blade are compared in the Fig .20. The magnitude of twist angle for the optimized blade is less than the magnitude of twist angle for the old blade. Decreasing twisted angle causes a change in angle of attack in each section of the blade and leads to an increase in output power.

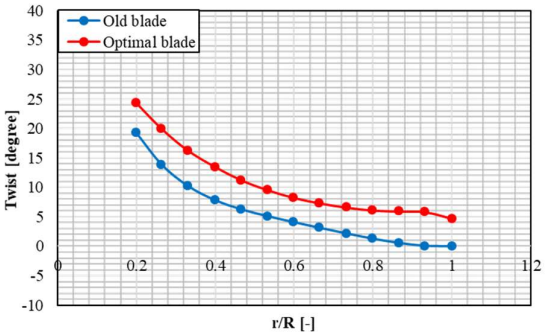

Fig. 20. The twisted angle of the optimized blade compared to the old blade

As can be seen in Fig. 21, the output power of the ducted fan with the optimal blade is higher than the old blade. According to the relation between power and velocity, the increase in the output power at higher velocities is more than the increase in the power in the lower velocities. The reported results indicate a ten percentages increase in the duct fan output.

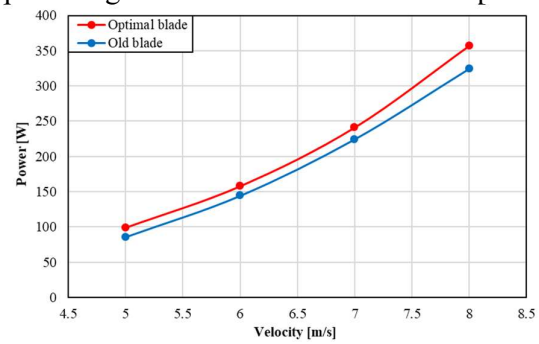

Fig. 21. The power curve of the ducted fan with the optimal blade and the old blade

Finally, it should be noted that an important key that could be considered is the structural analysis in design and optimization of a ducted fan. In this study, structural aspects have not been considered and only aerodynamic optimizations are conducted.

Conclusion

In this study, the surface vorticity method provides a powerful technique in modeling the potential flow around bodies with arbitrary shape. Viscous effects are not taken into account with the proposed model while having a significant role in the analysis of a ducted fan. These effects could cause separation from the duct and decrease the low-pressure region behind the rotor. Thereby, the present method is a handy tool for calculating the effects of shroud/duct on the performance of the fan, and it can be used for pre-designing ducted horizontal axis fans. The proposed model requires only lift and drag coefficients as input parameters. Therefore, the present method requires considerably less computational time than the CFD method. Also, to improve the efficiency of the duct fan, the aerodynamic optimization of the fan blade geometry has

been carried out using the particle aggregation method that is taken from the group movement of birds. The length of the chord and the twisted angle of the various sections of the blade are considered as variable parameters and the maximum output power as the objective function in 3D optimization of the fan. Using the optimized geometry for the fan, the reported results indicate a 10% increase in the duct fan output.

References

[1] G. Lilley, W. Rainbird. A preliminary report on the design and performance of ducted windmills. College of Aeronautics Cranfield1956.
[2] M.O.L. Hansen, N.N. Sørensen, R. Flay. Effect of placing a diffuser around a wind turbine. Wind Energy. 3 (2000) 207-13.
[3] O.d. Vries. Fluid dynamic aspects of wind energy conversion. DTIC Document1979.
[4] F.A. Al-Sulaiman, B.S. Yilbas. Thermoeconomic analysis of shrouded wind turbines. Energy Conversion and Management. 96 (2015) 599-604.
[5] P.T. Hoopen. A Literature Study and Experimental Investigation of a Diffuser Augemented Wind Turbine; In the Preparation of the Final Msc. Thesis Work2009.
[6] D.G. Phillips. An investigation on diffuser augmented wind turbine design. ResearchSpace@ Auckland2003.
[7] K. Foreman. Preliminary design and economic investigations of Diffuser-Augmented Wind Turbines (DAWT). Grumman Aerospace Corp., Bethpage, NY (USA). Research Dept.1981.
[8] O. Igra. Research and development for shrouded wind turbines. Energy Conversion and Management. 21 (1981) 13-48.
[9] L. Stipa. Ala a turbina. L'Aerotecnica. (1931) 923-53.
[10] L. Kort. Der neue düsenschrauben-antrieb. Werft, Reederei und Hafen. 15 (1934) 41-3.
[11] J. Van Manen. Recent research on propellers in nozzles. International Shipbuilding Progress. 4 (1957) 395-424.
[12] J. Van Manen, A. Superina. The design of screw-propellers in nozzles. International Shipbuilding Progress. 6 (1959) 95-113.
[13] J. Van Manen. Effect of radial load distribution on the performance of shrouded propellers. International Shipbuilding Progress. 9 (1962) 185-96.
[14] J. Van Manen. Analysis of ducted propeller design. Transaction SNAME. 74 (1966) 522.
[15] M.W.C. Oosterveld. Wake adapted ducted propellers. 1970.
[16] F. Horn. Beitrag zur theorie ummantelter schiffsschrauben. Jahrbuch der schiffbautechnischen Gesellschaft. (1940) 106-87.
[17] F. Horn, H. Amtsberg. Entwurf von schiffsdüsen systemen (kortdüsen). Jahrbuch der schiffbautechnischen Gesellschaft. 44 (1950) 141-206.
[18] W. Kruger. On wind tunnel tests and computations concerning the problem of shrouded propellers. (1949).
[19] A. Ko, O. Ohanian, P. Gelhausen. Ducted fan UAV modeling and simulation in preliminary design. AIAA modeling and simulation technologies conference and exhibit2007. p. 6375.
[20] H. Zhao, C. Bil. Aerodynamic design and analysis of a vtol ducted-fan uav. 26th AIAA Applied Aerodynamics Conference2008. p. 7516.
[21] A.I. Abrego, R.W. Bulaga. Performance study of a ducted fan system. AHS Aerodynamics, Aeroacoustic, Test and Evaluation Technical Specialist Meeting2002.
[22] J. Ahn, K. Lee. Performance prediction and design of a ducted fan system. 40th AIAA/ASME/SAE/ASEE Joint Propulsion Conference and Exhibit2004. p. 4196.
[23] J.E. Kerwin, S.A. Kinnas, J.-T. Lee, W.-Z. Shih. A surface panel method for the hydrodynamic analysis of ducted propellers. Massachusetts Inst of Tech Cambridge Dept of Ocean Engineering1987.
[24] M. Hughes. Implementation of a special procedure for modeling the tip clearance flow in a panel method for ducted propellers. Proceedings of the Propellers/Shafting'97 Symposium1997.
[25] J. Baltazar, D. Rijpkema, J. Falcao de Campos, J. Bosschers. A comparison of panel method and RANS calculations for a ducted propeller system in open-water. Third International Symposium on Marine Propulsors (SMP2013), Launceston, Tasmania, Australia2013.
[26] L. Yu, M. Greve, M. Druckenbrod, M. Abdel-Maksoud. Numerical analysis of ducted propeller performance under open water test condition. Journal of marine science and technology. 18 (2013) 381-94.
[27] R. Lind, J. Nathman, I. Gilchrist. Ducted Rotor Performance Calculations and Comparison with Experimental Data. 44th AIAA aerospace sciences meeting and exhibit2006. p. 1069.
[28] P. Martin, C. Tung. Performance and flowfield measurements on a 10-inch ducted rotor vtol uav. Army Research Development and Engineering Command Moffett Field CA Aviation, 2004.
[29] W. Graf, J. Fleming, W. Ng. Improving ducted fan UAV aerodynamics in forward flight. 46th AIAA aerospace sciences meeting and exhibit2008. p. 430.
[30] C. He, H. Xin. An unsteady ducted fan model for rotorcraft flight simulation. Annual froum proceedings-American Helicopter Society. INC2006. p. 1081.
[31] W.J.M. Rankine. On the mechanical principles of the action of propellers. Transactions of the Institution of Naval Architects. 6 (1865).
[32] R.E. Froude. On the part played in propulsion by differences of fluid pressure. Trans Inst Naval Architects. 30 (1889) 390.
[33] J.T. Conway. Analytical solutions for the actuator disk with variable radial distribution of load. Journal of Fluid Mechanics. 297 (1995) 327-55.
[34] H. Dickmann, J. Weissinger. Beitrag zur theorie optimaler dusenchrauben (kortdusen). Schiffbautrchn. 49 (1955) 452-86.
[35] L.A. Van Gunsteren. A contribution to the solution of some specific ship propulsion problems: A reappraisal of momentum theory. (1973).
[36] I. Gibson, R. Lewis. Ducted propeller analysis by surface vorticity and actuator disk theory. Proceedings of the Symposium on Ducted Propeller Royal Institute of Naval Architects1973.

[37] J. Falcao de Campos. On the calculation of ducted propeller performance in axisymmetric flows. (1983).
[38] H.R. Chaplin Jr. A method for numerical calculation of slipstream contraction of a shrouded impluse disc in the static case with application to other axisymmetric potential flow problems. Catholic University of merica Washington DC,1964.
[39] F. Çelik, M. Güner, S. Ekinci. An approach to the design of ducted propeller. Scientia Iranica Transaction B, Mechanical Engineering. 17 (2010) 406.
[40] S. Widnall. Potential Flow Calculations of Axisymmetric Ducted Wind Turbines. (2009).
[41] R. Lewis. Vortex element methods for fluid dynamic analysis of engineering systems. J Fluid Mech. 239 (1992) 720-3.
[42] E. Martensen. Die Berechnung der Druckverteilung an dicken Gitterprofilen mit Hilfe von Frodholmschen Integralgleichungen zweiter Art1959.
[43] R. Lewis. Surface vorticity modelling of separated flows from two-dimensional bluff bodies of arbitrary shape. Journal of Mechanical Engineering Science. 23 (1981) 1-12.
[44] L. Prandtl. Verhandlungen des dritten internationalen Mathematiker-Kongresses. Heidelberg, Leipeizig. (1904) 484-91.
[45] R. Lewis. Vortex element methods for fluid dynamic analysis of engineering systems. Cambridge Univ Press2003.
[46] C. Xu. Kutta condition for sharp edge flows. Mechanics research communications. 25 (1998) 415-20.
[47] J. Kennedy, R. Eberhart. Particle swarm optimization (PSO). Proc IEEE International Conference on Neural Networks, Perth, Australia1995. pp. 1942-8.
[48] X.-S. Yang. Nature-inspired optimization algorithms. Elsevier2014.
[49] D. Zou, S. Li, Z. Li, X. Kong. A new global particle swarm optimization for the economic emission dispatch with or without transmission losses. Energy Conversion and Management. 139 (2017) 45-70.
[50] J.C. Bansal, P. Singh, M. Saraswat, A. Verma, S.S. Jadon, A. Abraham. Inertia weight strategies in particle swarm optimization. Nature and Biologically Inspired Computing (NaBIC), 2011 Third World Congress on. IEEE2011. pp. 633-40.
[51] Y. Shi, R. Eberhart. Parameter selection in particle swarm optimization. Evolutionary programming VII. Springer1998. pp. 591-600.
[52] F. van Dorst, W. Energy. An Improved Rotor Design for a Diffuser Augmented Wind Turbine. Master's Thesis, TU Delft2011.
[53] P. Ten Hoppen. An experimental and computational investigation of a diffuser augmented wind turbine. M. Sc. Thesis, Delft University of Technology, Delft, The Netherlands2009.
[54] T. Burton, D. Sharpe, N. Jenkins, E. Bossanyi. Wind energy handbook. John Wiley & Sons2001.